AEROELASTIC ANALYSIS OF DISTRIBUTED ELECTRIC PROPULSION FLEXIBLE WINGS

Samet T. Dede[1], Ali Tatar[1,2], Djamel Rezgui[1] and Jonathan E. Cooper[1]

[1] University of Bristol, School of Civil, Aerospace and Design Engineering
Queen's Building, University Walk
Bristol BS8 1TR, United Kingdom
st.dede@bristol.ac.uk
ali.tatar@bristol.ac.uk
djamel.rezgui@bristol.ac.uk
j.e.cooper@bristol.ac.uk

[2] Istanbul Technical University, Faculty of Aeronautics and Astronautics
Ayazaga Campus, 34469, Maslak/Istanbul, Turkey
tataral@itu.edu.tr

Keywords: aeroelasticity, distributed electric propulsion, wing flutter, whirl flutter

Abstract: There is much current emphasis on the development of alternative aircraft propulsion technologies to enable much reduced, and eventually, net-zero in-flight commercial aircraft emissions. The success of this goal is not simply dependent upon the advancements in electric or hydrogen-powered propulsion systems, but also on how to integrate them into the aircraft structures. It is likely that distributed electric propulsion (DEP) configurations featuring small engines spaced across the wing will be the most viable solution. However, the adoption of these novel aircraft wing configurations might initiate the early onset of two potential aeroelastic instabilities: wing flutter and whirl flutter, which must be addressed in the early design stages of DEP aircraft wings. The main aim of this study is to create and evaluate a representative low-order aeroelastic coupled wing-propeller model for parametric aeroelastic studies that can be used in the flutter analysis at the early design stages. An aeroelastic numerical model was developed in MATLAB to analyse the aeroelastic behaviour of a coupled flexible cantilever wing with a variable number of flexibly mounted propellers/rotors. Reed's model is employed to model the propeller dynamics, with the structural model of the wing being derived through the assumed-mode Rayleigh-Ritz method. The aerodynamic model of the wing was obtained from a combination of the modified strip theory and Theodorsen's unsteady aerodynamic theory. The proposed coupled aeroelastic model can successfully estimate both wing and whirl flutter in DEP wings through validations with results from the literature. The model was then used for several parametric analyses investigating the effects of propeller spanwise position, advance ratio and rotor radius on the stability of the integrated wing-propeller system. The parametric studies demonstrated that advance ratio and rotor radius have a significant effect on the stability of the coupled wing-propeller model. It was found that increasing the advance ratio has a destabilizing effect, whereas increasing the rotor radius has a stabilizing effect.

1 INTRODUCTION

To decrease in-flight emissions in commercial aviation, there has been a significant focus on the idea of hybrid or fully electric aircraft in recent times [1, 2]. Unlike conventional aircraft powered by gas turbine engines, electric aircraft generate the necessary lift and thrust using propellers distributed along the wingspan, known as Distributed Electric Propulsion (DEP). Such a configuration enables zero-emission propulsion using multiple electric motors. Recent examples include the NASA X-57 Maxwell and DLR electric regional aircraft concepts, as seen in Figure 1. Owing to the current constraints in battery technologies, DEP aircraft typically feature high aspect ratio wings to enhance the aerodynamic efficiency and minimize the weight of the aircraft [3].

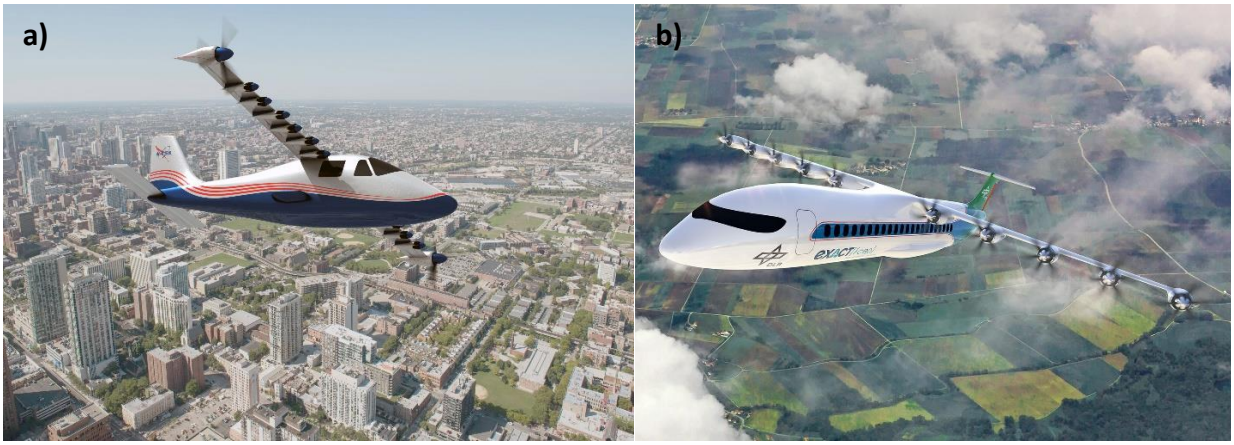

Figure 1: Examples of Distributed Electric Propulsion Aircraft
a) NASA X-57 Maxwell [4], b) DLR EXACT [5]

These novel aircraft wing configurations bring about the possibility of aeroelastic instabilities. Whirl flutter in particular occurs on aircraft with a flexibly attached propeller, and is defined by a diverging spiral motion caused by the precession of the propeller. Unlike classical wing flutter, which is caused by the interaction of aerodynamic, elastic, and inertial forces, whirl flutter is a result of the interplay between aerodynamic and gyroscopic forces acting on the propeller [6]. The onset of wing flutter or propeller whirl flutter can result in serious damage to aircraft structures and even fatal accidents. Hence, it is crucial to account for these aeroelastic instabilities during the initial design stages of DEP aircraft wings.

Dynamic aeroelastic instabilities have been extensively studied in the context of classical wing flutter and propeller whirl flutter. For classical wing flutter, a structural model of a flexible wing is employed, coupled with an aerodynamic model being represented by suitable unsteady aerodynamics theories, such as the strip theory or Doublet-Lattice-Method (DLM). The classical whirl flutter theory is presented for a flexibly mounted rigid propeller in pitch and yaw in [7-10]. Additionally, the aerodynamics of the propeller is established based on the blade geometry for propellers operating under windmilling conditions in both pitch and yaw motions [11, 12]. For a coupled wing-propeller model, Bennett and Bland [10] delivered an analytical approach and compared it with experimental data.

However, a limited number of investigations on the aeroelastic behaviour of DEP wings have been conducted, yet there is still potential for additional investigations. To understand the effect of propellers on the aeroelastic behaviour of the wing, a general methodology is also described in

[13]. Amoozgar et al. [14] devised a method to incorporate the influence of propellers on wing aeroelastic characteristics by representing the electric propeller as a concentrated mass on the wing and included the thrust force generated by the propeller as a follower force when formulating the aeroelastic governing equations. Heeg et al. [15] extensively investigated the stability of propeller whirl flutter during the development of the NASA X-57 Maxwell aircraft through multibody dynamics simulation tools. Böhnisch et al. [16-18] introduced an aeroelastic model to examine the whirl flutter of DEP wings and conducted various parametric studies on DEP wings. In their model, the propellers are attached to a flexible wing through rigid pylons that can move in both pitch and yaw directions. Recently, Tamer and Tatar [19] proposed a minimum complexity model for the aeroelastic analysis of wing-propeller systems. Their study primarily shows how rapidly the model can be updated during various parametric studies on DEP wings. Although the majority of these studies are based on finite element and finite element volume methods, which have advantages such as more accurate representation of the wing, lower-order models can still be useful for rapid analysis, optimization purposes, or real-time simulations.

None of the aforementioned studies addressed the aeroelastic analysis of an electric aircraft wing featuring a DEP configuration using the Rayleigh-Ritz approach, which can offer several advantages due to its easy usage and reduced computational time. It maintains a large portion of accuracy, especially if enough assumed modes are used. Therefore, this study aims to create and evaluate a representative low-order aeroelastic coupled wing-propeller model in parametric aeroelastic studies that can be used in flutter analysis at the early design stages. The analysis is then used to examine the aeroelastic stability of a DEP aircraft wing. A systematic parameter analysis is conducted by changing the propeller position and propeller parameters such as advance ratio and rotor radius, identifying their impact on the stability of a representative DEP wing. The propeller parameters above are some of the major parameters that can influence whirl flutter. Their impact on an isolated propeller on a rigid wing has been well understood, whereas less research has considered the case of a propeller flexibly attached to a flexible wing and the resulting aeroelastic instabilities of DEP wings. This study presents a coupled aeroelastic model, which can be used in the preliminary design stages of DEP wings and discusses the results of several parametric analyses conducted on the stability of DEP wings.

For this study, a baseline wing and propeller model are defined and used for creating a coupled propeller-wing model. An aeroelastic numerical model is developed in MATLAB to analyse the aeroelastic behaviour of the coupled system with no aerodynamic interference effects between the wing and propeller for a freestream velocity range. Reed's model is used to represent the propeller dynamics, while the wing's structural model is derived using the assumed-mode Rayleigh-Ritz method. The aerodynamic model of the wing is obtained by combining the modified strip theory with Theodorsen's unsteady aerodynamics theory. The developed coupled aeroelastic model is subsequently used for several parametric analyses. The key findings are summarised in section 4.

2 MATHEMATICAL MODELLING

2.1 Derivation of Aeroelastic Equations of Motion of Standalone Wing

The simple rectangular cantilever wing with semi-span s and chord c considered to derive the aeroelastic equations of motion has bending rigidity EI and torsional rigidity GJ. The equations of motion of a wing are composed of the structural model and the aerodynamic model. In this study, the structural model of the wing is represented by the Rayleigh-Ritz method, which is applied to

model the deformation of the two-dimensional wing system. At any point along the wing, the deformation $z(x,y,t)$ caused by bending and twisting is expressed by the following series [20]

$$z(x,y,t) = \sum_{i=1}^{N} \psi_i(x,y) q_i(t) \tag{1}$$

In this series, $\psi_i(x,y)$ represents one of N assumed deformation shapes, while $q_i(t)$ denotes the coefficients of generalized coordinates of the unknown magnitude. As the cantilever wing is clamped at the root, the following fixed boundary conditions are imposed.

$$z = \dot{z} = 0 \;\; at \;\; y = 0 \tag{2}$$

Two mode shapes (one bending and one torsion) are assumed. For bending and twisting about an elastic axis,

$$z(x,y,t) = h + (x - x_f)\alpha \tag{3}$$

where x_f is the chord-wise position of the elastic axis from the leading edge. The bending h and torsion α deflections are expressed through the Rayleigh-Ritz in terms of mode shapes and generalized coordinates by

$$h(y,t) = \left(\frac{y}{s}\right)^2 q_h \qquad\qquad \alpha(y,t) = \left(\frac{y}{s}\right) q_\alpha \tag{4}$$

Using these generalized coordinates $q_i(t)$ and omitting the damping term, Lagrange's equations can be then expressed as

$$\frac{d}{dt}\left(\frac{\partial T}{\partial \dot{q}_i}\right) - \frac{\partial T}{\partial q_i} + \frac{\partial U}{\partial q_i} + \frac{\partial D}{\partial \dot{q}_i} = Q_i \qquad i = h, \alpha \tag{5}$$

where Q_i denotes the generalized forces. T is the kinetic energy, U is the potential energy, and D is the dissipation or damping function. The equations of motion of the wing can be derived through Lagrange's equations. The kinetic energy of the wing is

$$T = \frac{m}{2}\int_0^s \int_0^c (\dot{z})^2 \, dx \, dy$$

$$T = \frac{m}{2}\int_0^s \int_0^c \left(\left(\frac{y}{s}\right)^2 \dot{q}_h + \left(\frac{y}{s}\right)(x - x_f)\dot{q}_a\right)^2 dx \, dy$$

where m is mass per unit area.

$$\left(\frac{\partial T}{\partial \dot{q}_h}\right) = m\int_0^s \int_0^c \left(\left(\frac{y}{s}\right)^4 \dot{q}_h + \left(\frac{y}{s}\right)^3 (x - x_f)\dot{q}_a\right) dx \, dy \tag{6}$$

$$\frac{d}{dt}\left(\frac{\partial T}{\partial \dot{q}_h}\right) = m\left[\frac{sc}{5}\ddot{q}_h + \frac{s}{4}\left(\frac{c^2}{2} - cx_f\right)\ddot{q}_a\right]$$

$$\left(\frac{\partial T}{\partial \dot{q}_a}\right) = m\int_0^s \int_0^c \left(\left(\frac{y}{s}\right)^3 (x - x_f)\dot{q}_h + \left(\frac{y}{s}\right)^2 (x - x_f)^2 \dot{q}_a\right) dx \, dy$$

$$\frac{d}{dt}\left(\frac{\partial T}{\partial \dot{q}_a}\right) = m\left[\frac{s}{4}\left(\frac{c^2}{2} - cx_f\right)\ddot{q}_h + \frac{s}{3}\left(\frac{c^3}{3} - c^2 x_f + cx_f{}^2\right)\ddot{q}_a\right]$$

The potential energy caused by the strain energy effect over the wing is expressed as

$$U = \frac{1}{2}\int_0^s EI\left(\frac{\partial^2 z}{\partial y^2}\right)^2 dy + \frac{1}{2}\int_0^s GJ\left(\frac{\partial a}{\partial y}\right)^2 dy$$

$$U = \frac{1}{2}\int_0^s EI\left(\frac{2}{s^2}q_h\right)^2 dy + \frac{1}{2}\int_0^s GJ\left(\frac{1}{s}q_a\right)^2 dy \tag{7}$$

$$\left(\frac{\partial U}{\partial q_h}\right) = \frac{4EI}{s^3}q_h \qquad \left(\frac{\partial U}{\partial q_a}\right) = \frac{GJ}{s}q_a$$

Therefore, structural equations become

$$m\begin{bmatrix} \frac{sc}{5} & \frac{s}{4}\left(\frac{c^2}{2} - cx_f\right) \\ \frac{s}{4}\left(\frac{c^2}{2} - cx_f\right) & \frac{s}{3}\left(\frac{c^3}{3} - c^2 x_f + cx_f{}^2\right) \end{bmatrix}\begin{bmatrix}\ddot{q}_h \\ \ddot{q}_a\end{bmatrix} + \begin{bmatrix}\frac{4EI}{s^3} & 0 \\ 0 & \frac{GJ}{s}\end{bmatrix}\begin{bmatrix}q_h \\ q_a\end{bmatrix} = \begin{bmatrix}0 \\ 0\end{bmatrix} \tag{8}$$

In this study, the aerodynamic model is represented by a combination of the simplified Theodorsen method with the aerodynamic strip theory, incorporating unsteady aerodynamic derivative $M_{\dot{a}}$ to account for pitch damping. $M_{\dot{a}} = -1.2$ is incorporated into the moment equation to enhance the model's flutter behaviour predictions [20]. To determine the total lift and moment, the lift (dL) and moment (dM) for each strip dy are provided in Equation (9). With the assumption of constant $M_{\dot{a}}$, this model remains unaffected by changes in the reduced frequency and thus

$$dL = \frac{1}{2}\rho V^2 c a_w\left(a + \frac{\dot{z}}{V}\right) \qquad dM = \frac{1}{2}\rho V^2 c^2\left[e a_w\left(a + \frac{\dot{z}}{V}\right) + M_{\dot{a}} c\frac{\dot{a}}{4V}\right] \tag{9}$$

where a_w is the two-dimensional lift curve slope and e denotes the eccentricity ratio between the elastic axis and the aerodynamic centre. The incremental work (W) done by these forces and moments can be written as

$$\delta W = \int_0^s\left[dL\left(-\left(\frac{y}{s}\right)^2\delta q_h\right) + dM\left(\left(\frac{y}{s}\right)\delta q_a\right)\right] \tag{10}$$

With the addition of the incremental work done (W) by the aerodynamic forces, the generalised forces are specified as

$$Q_{q_h} = \frac{\partial(\delta W)}{\partial(\delta q_h)} = -\int_0^s y^2 dL = -\frac{1}{2}\rho V^2 c a_w\int_0^s\left(\left(\frac{y}{s}\right)^4\frac{\dot{q}_h}{V} + \left(\frac{y}{s}\right)^3 q_a\right)dy$$

$$Q_{q_h} = -\frac{1}{2}\rho V^2 c a_w \left(\frac{s}{5V}\dot{q}_h + \frac{s}{4}q_a\right) \tag{11}$$

$$Q_{q_a} = \frac{\partial(\delta W)}{\partial(\delta q_a)} = \int_0^s \left(\frac{y}{s}\right) dM = \frac{1}{2}\rho V^2 c^2 \int_0^s \left[e a_w \left(\left(\frac{y}{s}\right)^3 \frac{\dot{q}_h}{V} + \left(\frac{y}{s}\right)^2 q_a\right) + M_{\dot{a}} c \left(\frac{y}{s}\right)^2 \frac{\dot{q}_a}{4V}\right] dy$$

$$Q_{q_a} = \frac{1}{2}\rho V^2 c^2 \left[e a_w \left(\frac{s}{4V}\dot{q}_h + \frac{s}{3}q_a\right) + M_{\dot{a}} c \left(\frac{s}{12V}\dot{q}_a\right)\right]$$

Hence, aerodynamic equations become

$$\rho V \begin{bmatrix} -\frac{csa_w}{10} & 0 \\ \frac{c^2 sea_w}{8} & \frac{c^3 s M_{\dot{a}}}{24} \end{bmatrix} \begin{bmatrix} \dot{q}_h \\ \dot{q}_a \end{bmatrix} + \rho V^2 \begin{bmatrix} 0 & -\frac{csa_w}{8} \\ 0 & \frac{c^2 sea_w}{6} \end{bmatrix} \begin{bmatrix} q_h \\ q_a \end{bmatrix} \tag{12}$$

Implementing Lagrange's equations to the expressions derived for the kinetic and potential energy of the wing yields the aeroelastic equations of motion of the wing given in Equation (13).

$$M\ddot{q} + (\rho V C_{aero} + C_{structural})\dot{q} + (\rho V^2 K_{aero} + K_{structural})q = 0 \tag{13}$$

where q is the vector of generalized coordinates, M is the mass matrix, C_{aero} is the aerodynamic damping matrix, $C_{structural}$ is the structural damping matrix, $K_{structural}$ is the structural stiffness matrix and K_{aero} is the aerodynamic stiffness matrix. Equation (13) can be written in matrix form as

$$m\begin{bmatrix} \frac{sc}{5} & \frac{s}{4}\left(\frac{c^2}{2} - cx_f\right) \\ \frac{s}{4}\left(\frac{c^2}{2} - cx_f\right) & \frac{s}{3}\left(\frac{c^3}{3} - c^2 x_f + c{x_f}^2\right) \end{bmatrix} \begin{bmatrix} \ddot{q}_h \\ \ddot{q}_a \end{bmatrix} + \rho V \begin{bmatrix} \frac{csa_w}{10} & 0 \\ -\frac{c^2 sea_w}{8} & -\frac{c^3 s M_{\dot{a}}}{24} \end{bmatrix} \begin{bmatrix} \dot{q}_h \\ \dot{q}_a \end{bmatrix}$$
$$+ \left\{ \rho V^2 \begin{bmatrix} 0 & \frac{csa_w}{8} \\ 0 & -\frac{c^2 sea_w}{6} \end{bmatrix} + \begin{bmatrix} \frac{4EI}{s^3} & 0 \\ 0 & \frac{GJ}{s} \end{bmatrix} \right\} \begin{bmatrix} q_h \\ q_a \end{bmatrix} = \begin{bmatrix} 0 \\ 0 \end{bmatrix} \tag{14}$$

Equation (14) is now in state-space form, which can be rearranged as

$$\begin{bmatrix} \dot{q} \\ \ddot{q} \end{bmatrix} = \begin{bmatrix} 0 & I \\ -M^{-1}(K_{structural} - K_{aero}) & -M^{-1}(C_{structural} - C_{aero}) \end{bmatrix} \begin{bmatrix} q \\ \dot{q} \end{bmatrix} \tag{15}$$

where $\mathbf{0}$ and $\boldsymbol{I}$ denote two by two zero and identity matrices, respectively. The structural damping of the wing is neglected since $C_{structural}$ is set to zero.

The Jacobian matrix is then written as

$$J = \begin{bmatrix} 0 & I \\ -M^{-1}(K_{strucutal} - K_{aero}) & -M^{-1}(C_{structural} - C_{aero}) \end{bmatrix} \tag{16}$$

The frequency and damping of the system can be calculated from the eigenvalues of the Jacobian matrix, while the mode shapes can be obtained from the corresponding eigenvectors. The undamped natural frequency ω and damping ratio ζ for a given mode are derived through the real and imaginary parts of its eigenvalue λ, as given in Equation (17).

$$\omega = \sqrt{Re(\lambda)^2 + Im(\lambda)^2} \qquad \zeta = \frac{-Re(\lambda)}{\omega} \tag{17}$$

Increasing the number of terms incorporated into the model enhances the accuracy of the results. For two bending and two torsion assumed modes, the deflection can be represented as

$$z = \left(\frac{y}{s}\right)^2 q_{h1} + \left(\frac{y}{s}\right)^3 q_{h2} + \left(\frac{y}{s}\right)(x - x_f) q_{a1} + \left(\frac{y}{s}\right)^2 (x - x_f) q_{a2} \tag{18}$$

2.2 Derivation of Aeroelastic Equations of Motion of Standalone Propeller

The references [12, 21, 22] describe a basic model of an isolated propeller with two degrees of freedom. In this model, a rotor with radius R and angular velocity Ω, possessing a moment of inertia I_x about its rotational axis, is allowed to move in both pitch θ and yaw ψ about an effective pivot point with a moment of inertia I_n. The dynamics of the wing structure are represented by structural stiffnesses (K_θ, K_ψ) and structural damping (C_θ, C_ψ) in both pitch and yaw directions at the pivot point. The rotor is attached to the pivot point at a distance of aR. The schematic of the model is presented in Figure 2. Aerodynamic loads are calculated using the strip theory.

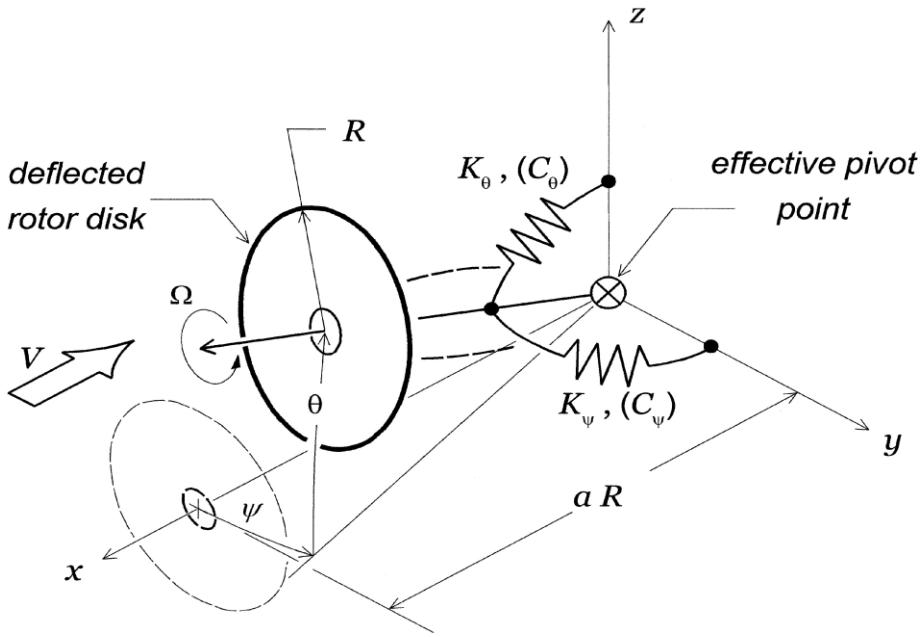

Figure 2: Schematic of Rotor-Nacelle Dynamic System [21]

The basic equations of motion for this rotor-nacelle dynamic system, as presented by Bielawa [21], can be expressed as

$$\begin{aligned} I_n\ddot{\theta} + C_\theta\dot{\theta} - I_x\Omega\dot{\psi} + K_\theta\theta &= M_\theta \\ I_n\ddot{\psi} + C_\psi\dot{\psi} + I_x\Omega\dot{\theta} + K_\psi\psi &= M_\psi \end{aligned} \tag{19}$$

where M_θ and M_ψ denote aerodynamic moments in pitch and yaw directions, respectively. The aeromechanical model of this dynamic system in matrix form can thus be defined as

$$\begin{bmatrix} I_n & 0 \\ 0 & I_n \end{bmatrix}\begin{bmatrix} \ddot{\theta} \\ \ddot{\psi} \end{bmatrix} + \begin{bmatrix} C_\theta & -I_x\Omega \\ I_x\Omega & C_\psi \end{bmatrix}\begin{bmatrix} \dot{\theta} \\ \dot{\psi} \end{bmatrix} + \begin{bmatrix} K_\theta & 0 \\ 0 & K_\psi \end{bmatrix}\begin{bmatrix} \theta \\ \psi \end{bmatrix} = \begin{bmatrix} M_\theta \\ M_\psi \end{bmatrix} \tag{20}$$

There are two aerodynamic forces and moments acting on the propeller hub, which are formulated as

$$\begin{aligned} L_y &= \frac{N_B}{2}K_\alpha\left(A_1'\psi - aA_1\frac{\dot{\psi}}{\Omega} + A_2\frac{\dot{\theta}}{\Omega}\right) \\ L_z &= \frac{N_B}{2}K_\alpha\left(A_1'\theta - aA_1\frac{\dot{\theta}}{\Omega} - A_2\frac{\dot{\psi}}{\Omega}\right) \\ M_y &= \frac{N_B}{2}K_\alpha R\left(A_2'\psi - aA_2\frac{\dot{\psi}}{\Omega} + A_3\frac{\dot{\theta}}{\Omega}\right) \\ M_z &= \frac{N_B}{2}K_\alpha R\left(A_2'\theta - aA_2\frac{\dot{\theta}}{\Omega} - A_3\frac{\dot{\psi}}{\Omega}\right) \end{aligned} \tag{21}$$

where N_B and a are the number of blades and pivot length to rotor radius ratio.

$$K_a = \frac{1}{2}\rho C_{l\alpha}R^4\Omega^2 \tag{22}$$

where ρ and $C_{l\alpha}$ denote the density of air and blade lift slope, respectively. The A_i terms are written as

$$\begin{aligned} A_1 &= \int_0^1 \frac{c}{R}\frac{\mu^2}{\sqrt{\mu^2+\eta^2}}d\eta \qquad & A_1' &= \mu A_1 \\ A_2 &= \int_0^1 \frac{c}{R}\frac{\mu\eta^2}{\sqrt{\mu^2+\eta^2}}d\eta \qquad & A_2' &= \mu A_2 \\ A_3 &= \int_0^1 \frac{c}{R}\frac{\eta^4}{\sqrt{\mu^2+\eta^2}}d\eta \qquad & A_3' &= \mu A_3 \end{aligned} \tag{23}$$

where $\mu = \frac{J}{\pi} = \frac{V}{\Omega R}$ is the advance ratio and $\eta = \frac{r}{R}$. c denotes the blade chord. The propeller pitching and yawing moments around the pivot point can be defined such that

$$\begin{aligned} M_\theta &= -M_y + aRL_z \\ M_\psi &= M_z + aRL_y \end{aligned} \tag{24}$$

which leads to

$$\begin{aligned} M_\theta &= \frac{N_B}{2}K_\alpha R\left[-(A_3 + a^2A_1)\frac{\dot{\theta}}{\Omega} - A_2'\psi + aA_1'\theta\right] \\ M_\psi &= \frac{N_B}{2}K_\alpha R\left[-(A_3 + a^2A_1)\frac{\dot{\psi}}{\Omega} + A_2'\theta + aA_1'\psi\right] \end{aligned} \tag{25}$$

The aerodynamic damping (C_{aero}) and aerodynamic stiffness (K_{aero}) matrices derived from the above two aerodynamic moments about the pivot point are given as

$$C_{aero1} = -\frac{N_B}{2} K_\alpha R \frac{(A_3 + a^2 A_1)}{\Omega}$$

$$K_{aero1} = \frac{N_B}{2} K_\alpha R a A_1' \qquad K_{aero2} = \frac{N_B}{2} K_\alpha R A_2' \tag{26}$$

and hence the general aerodynamic model of the rotor-nacelle dynamic system is

$$\begin{bmatrix} C_{aero1} & 0 \\ 0 & C_{aero1} \end{bmatrix} \begin{bmatrix} \dot{\theta} \\ \dot{\psi} \end{bmatrix} + \begin{bmatrix} K_{aero1} & -K_{aero2} \\ K_{aero2} & K_{aero1} \end{bmatrix} \begin{bmatrix} \theta \\ \psi \end{bmatrix} = \begin{bmatrix} M_\theta \\ M_\psi \end{bmatrix} \tag{27}$$

Following the determination of the structural and aerodynamic models separately, the aeroelastic model of this dynamic system can be written as

$$\begin{bmatrix} I_n & 0 \\ 0 & I_n \end{bmatrix} \begin{bmatrix} \ddot{\theta} \\ \ddot{\psi} \end{bmatrix} + \begin{bmatrix} C_\theta & -I_x\Omega \\ I_x\Omega & C_\psi \end{bmatrix} \begin{bmatrix} \dot{\theta} \\ \dot{\psi} \end{bmatrix} + \begin{bmatrix} K_\theta & 0 \\ 0 & K_\psi \end{bmatrix} \begin{bmatrix} \theta \\ \psi \end{bmatrix} = \begin{bmatrix} C_{aero1} & 0 \\ 0 & C_{aero1} \end{bmatrix} \begin{bmatrix} \dot{\theta} \\ \dot{\psi} \end{bmatrix} + \begin{bmatrix} K_{aero1} & -K_{aero2} \\ K_{aero2} & K_{aero1} \end{bmatrix} \begin{bmatrix} \theta \\ \psi \end{bmatrix} \tag{28}$$

The stability of the linear system is evaluated by calculating its frequency and damping through eigenvalue analysis. For a mechanical system with damping and gyroscopic terms, solving the eigenvalue problem is more sophisticated because these terms bring the first derivatives of the generalized coordinates to the equations of motion. Therefore, the eigenvalue problem converts into a quadratic eigenvalue problem, which can be reduced to a first-order state-space model.

2.3 Derivation of Aeroelastic Equations of Motion of Wing with Single Propeller

The propeller-wing model integrates the previous two models by including relevant structural and aerodynamic coupling terms. The rotor and nacelle system that is discussed in subsection 2.2 assumes flexibly mounted engines on rigid wings. This assumption can be useful when investigating the influences of particular parameters on the whirl flutter. However, in general, the flexibility of the wing influences the dynamic characteristics of the entire system, which consequently influences the whirl flutter characteristics. Therefore, the effect of the wing flexibility is included in the equations of motion.

Lagrange's equations for the coupled wing-propeller model are provided in Equation (29). This model considers propeller pitch θ, propeller yaw ψ, propeller-wing attachment point displacement h_p and propeller-wing attachment point twist a_p which becomes

$$\frac{d}{dt}\left(\frac{\partial T}{\partial \dot{q}_i}\right) - \frac{\partial T}{\partial q_i} + \frac{\partial U}{\partial q_i} + \frac{\partial D}{\partial \dot{q}_i} = Q_i \qquad i = \theta, \psi, h_p, a_p \tag{29}$$

The equations of motion of the coupled wing-propeller model obtained through Lagrange's equations are given in Equation (30) and the terms in the equations of motion of the coupled model [23] are explained in [13, 23].

$$\begin{aligned} I_{\theta,p}\ddot{\theta} + K_\theta\theta + C_\theta\dot{\theta} + I_\Omega\Omega\dot{\psi} + S_{\theta,p}\ddot{h}_p + I_{\theta\alpha,p}\ddot{\alpha}_p &= Q_{\theta,p} \\ -I_\Omega\Omega\dot{\theta} + I_{\psi,p}\ddot{\psi} + K_\psi\psi + C_\psi\dot{\psi} - I_\Omega\Omega\dot{\alpha}_p &= Q_{\psi,p} \\ M_w\ddot{h} + S_{\theta,p}\ddot{\theta} + M_p\ddot{h}_p + S_{\alpha,p}\ddot{\alpha}_p + S_{\alpha,w}\ddot{\alpha} &= Q_{h,w} + Q_{h,p} \\ I_{\alpha,w}\ddot{\alpha} + S_{\alpha,w}\ddot{h} + I_{\theta\alpha,p}\ddot{\theta} + I_\Omega\Omega\dot{\psi} + S_{\alpha,p}\ddot{h}_p + I_{\alpha,p}\ddot{\alpha}_p &= Q_{\alpha,w} + Q_{\alpha,p} \end{aligned} \tag{30}$$

The propeller aerodynamic moments about the pivot point are given as

$$Q_{\theta,P} = M_Y + e_\theta F_Z$$
$$Q_{\psi,P} = M_Z - e_\psi F_Y \tag{31}$$

where e_θ and e_ψ are the distance between the propeller hub and elastic centres in pitch and yaw, respectively. The aerodynamic effect of propellers on the wing is considered by applying propeller aerodynamic loads onto the wing structural model so that

$$Q_{h,P} = F_Z$$
$$Q_{\alpha,P} = M_Y + e_\alpha F_Z \tag{32}$$

where e_α denotes the distance between the propeller hub and the propeller pivoting point and F_Y, F_Z, M_Y and M_Z are the aerodynamic forces and moments produced by the propeller.

$$F_Y = \frac{1}{2}\rho V^2 S' \left(C_{Y_\theta}\overline{\theta} + C_{Y_\psi}\overline{\psi} + C_{Y_q}\frac{\dot{\overline{\theta}}R}{V} + C_{Y_r}\frac{\dot{\overline{\psi}}R}{V} \right)$$
$$F_Z = \frac{1}{2}\rho V^2 S' \left(C_{Z_\theta}\overline{\theta} + C_{Z_\psi}\overline{\psi} + C_{Z_q}\frac{\dot{\overline{\theta}}R}{V} + C_{Z_r}\frac{\dot{\overline{\psi}}R}{V} \right) \tag{33}$$
$$M_Y = \rho V^2 S' R \left(C_{m_\theta}\overline{\theta} + C_{m_\psi}\overline{\psi} + C_{m_q}\frac{\dot{\overline{\theta}}R}{V} + C_{m_r}\frac{\dot{\overline{\psi}}R}{V} \right)$$
$$M_Z = \rho V^2 S' R \left(C_{n_\theta}\overline{\theta} + C_{n_\psi}\overline{\psi} + C_{n_q}\frac{\dot{\overline{\theta}}R}{V} + C_{n_r}\frac{\dot{\overline{\psi}}R}{V} \right)$$

The propeller forces and moments given above are determined employing the sixteen propeller stability derivatives, provided in [8, 10, 11], which are applicable under windmilling conditions. These derivatives explain how the forces and moments vary with the effective pitch and yaw angles. Due to the interaction with the wing, these effective pitch and yaw angles for the coupled model are specified as

$$\overline{\theta} = \theta + \alpha_p + \frac{e_\theta}{V}\dot{\theta} + \frac{e_\alpha}{V}\dot{\alpha}_p + \frac{1}{V}\dot{h}_p \qquad\qquad \overline{\psi} = \psi + \frac{e_\psi}{V}\dot{\psi} \tag{34}$$

and the generalized aerodynamic forces of the coupled model can be defined as

$$Q_\theta = Q_{\theta,P}$$
$$Q_\psi = Q_{\psi,P} \tag{35}$$
$$Q_h = Q_{h,P} + Q_{h,W}$$
$$Q_\alpha = Q_{\alpha,P} + Q_{\alpha,W}$$

With the combination of the expressions in the obtained generalized aerodynamic forces, a coupled aeroelastic wing-propeller model can be derived in matrix form, as provided in [13].

3 NUMERICAL ANALYSIS

3.1 Baseline Wing

The schematic of a baseline wing from [13] is illustrated in Figure 2 with the main parameters of the tapered wing outlined in Table 1. The elastic axis (EA) and centre of gravity (CG) are coincident and located at the wing mid-chord.

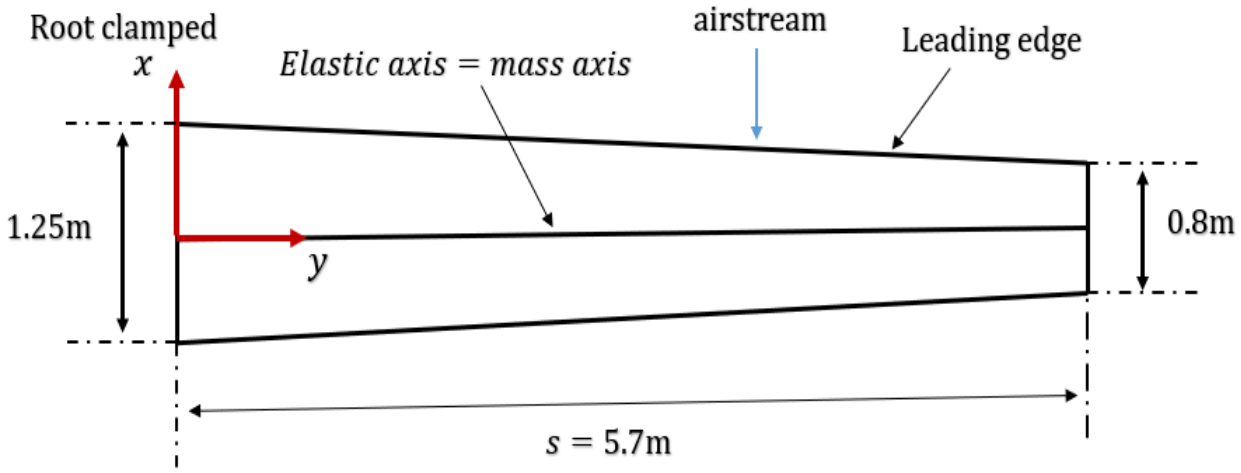

Figure 3: Schematic of baseline wing

Table 1: Baseline wing parameters

Wing Parameter	Value
Wing span [m]	11.4
Root chord [m]	1.25
Tip chord [m]	0.8
Mass per unit length [kg/m]	25
Aerodynamic centre [-]	25% chord
Elastic axis [-]	50% chord
Centre of gravity [-]	50% chord
Radius of Gyration about CG [-]	25% chord
Bending rigidity [Nm^2]	7E5
Torsional rigidity [Nm^2]	2E5
Lift curve slope [-]	2π
Density of air [kg/m^3]	0.96287

The structural model of the wing is based on the methodology presented in subsection 2.1. Table 2 compares the natural frequencies of the baseline wing. It is seen that there is a good agreement between the present study and the results achieved in the reference paper [13] in terms of natural frequencies.

Table 2: Comparison of natural frequencies of baseline wing

Mode	Present Study [Hz]	Reference Study [13] [Hz]	Deviation [%]
First Bending	2.88	2.88	0
First Torsion	16.68	16.68	0
Second Bending	18.06	18.06	0
Second Torsion	46.49	46.59	0.21
Third Bending	50.58	50.57	0.04

The first four wind-off mode shapes of the wing are also given in Figure 4. Since the mass axis and the elastic axis are coincident at the wing mid-chord axis, the wind-off mode shapes are composed of pure bending and pure torsion without coupling.

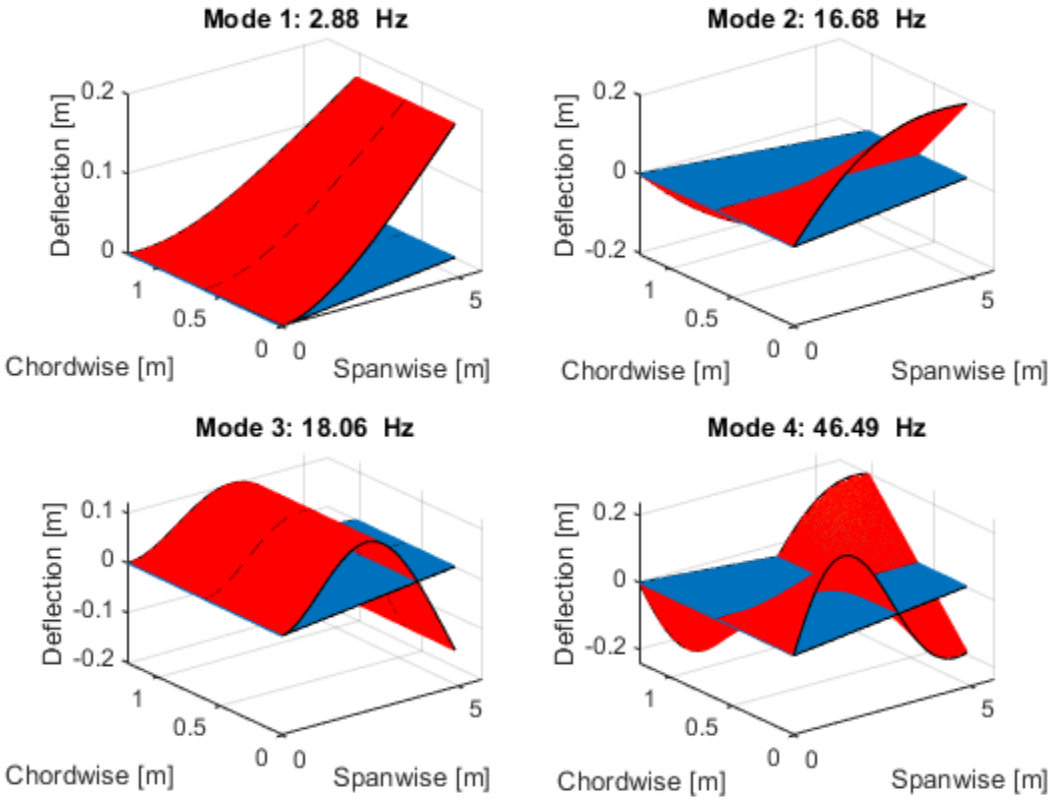

Figure 4: Wind-off mode shapes of baseline wing

The flutter speed and frequency of the wing are predicted by the methodology provided in subsection 2.1 and are tabulated in Table 3. The velocity-frequency and velocity-damping curves illustrated in Figure 5 demonstrate that the first torsional mode (flutter mode) is unstable due to interaction between the first torsion mode and the first bending mode, whereas divergence mode is the first bending mode.

Table 3: Comparison of aeroelastic results of baseline wing

Parameter	Present Study	Reference Study [13]	Deviation [%]
Flutter Speed	151.4 m/s	152 m/s	0.91
Flutter Frequency	8.41 Hz	8.08 Hz	4.08

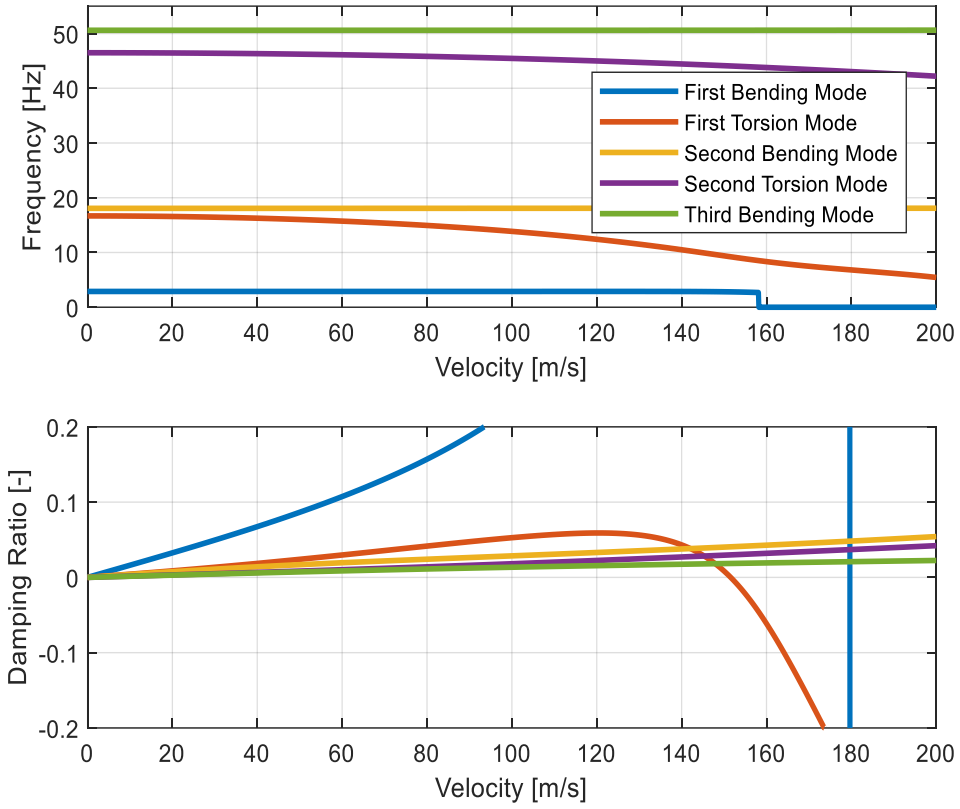

Figure 5: Variation of modal frequency and damping with freestream velocity of baseline wing

3.2 Baseline Propeller

A baseline propeller from [13] is represented by two concentrated masses: Rotor mass and motor-nacelle mass. The main parameters of this cruise propeller used in the NASA X-57 Maxwell electric aircraft are summarized in Table 4. It is assumed that the baseline propeller analysed in this study have fixed-pitch blades and operate under windmilling conditions. Hence, the propeller advance ratio remains constant and is determined based on the specified geometric collective pitch angle. The rotational speed of the propeller changes with the freestream velocity to sustain this advance ratio. The pitch and yaw motions of the isolated propeller are considered to be symmetric. In the current 2-DOF propeller model, the frequency and damping coefficient for propeller pitch and yaw motions are used for analysing the propeller's structural dynamics. The uncoupled pitch and yaw frequencies ensure to determine the pitch stiffness ($K_\theta = 7E4\ Nmrad^{-1}$) and yaw stiffness ($K_\psi = 7E4\ Nmrad^{-1}$). Additionally, the pitch and yaw damping coefficients are utilized to assess the structural damping of the nacelle.

Table 4: Baseline propeller parameters

Propeller Parameter	Value
Number of blades [-]	3
Rotor radius [m]	0.762
Rotor mass [kg]	8
Rotor position [m]	1.16
Motor & nacelle mass [kg]	35
Motor position [m]	0.86
Blade chord [m]	0.094
Advance ratio [-]	1.96
Pitch and yaw stiffness [Hz]	7
Pitch and yaw damping coefficient [-]	0.005

With the assumption that the baseline propeller is flexibly attached to a rigid wing, whirl flutter analysis is conducted using Reed's model in line with the methodology given in subsection 2.2. The whirl flutter speed and frequency of the baseline propeller are tabulated and compared with the results of the reference paper in Table 5.

Table 5: Comparison of aeroelastic results of baseline propeller

Parameter	Present Study	Reference Study [13]	Deviation [%]
Whirl Flutter Speed	223 m/s	221 m/s	0.91
Whirl Flutter Frequency	4.92 Hz	5 Hz	1.63

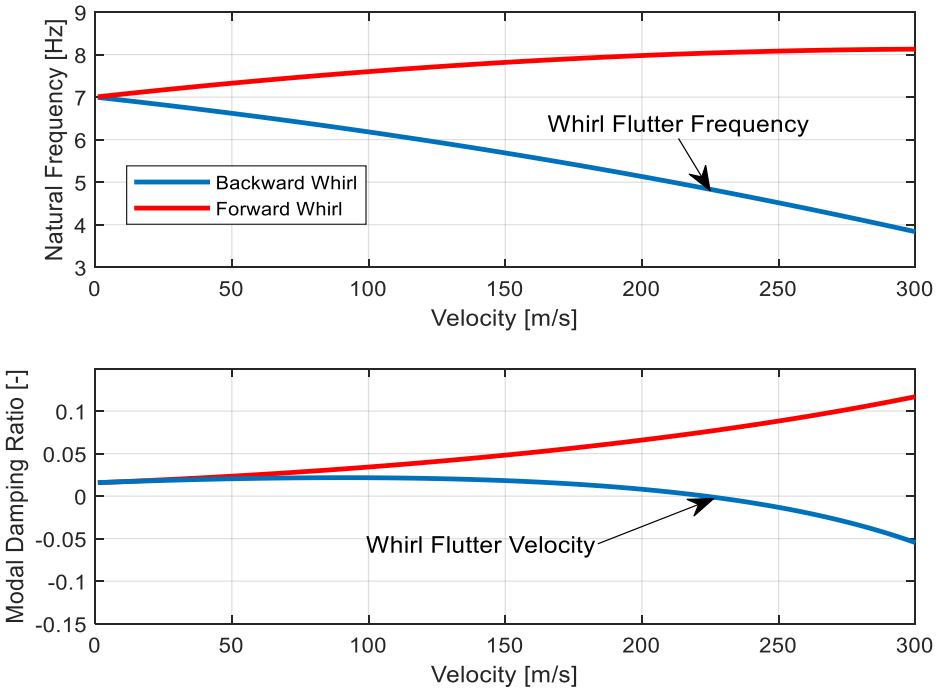

Figure 6: Variation of modal damping ratio and frequency with freestream velocity

The corresponding whirl flutter curves illustrated in Figure 6 indicate similar trend with the results gained in [13]. The corresponding whirl flutter curves illustrated in Figure 6 indicate similar trend with the results gained in [13]. The propeller's motion is characterized by two modes: a backward whirling mode and a forward whirling mode. Since the rigid propeller blades and rigid wings are assumed, the forward whirling mode is stable and becomes even more stable with growing airspeeds. Whirl flutter only develops in the backward whirling mode. The forward whirling mode has higher frequencies compared to the backward whirling mode. Since the advance ratio remains constant in this whirl flutter analysis, increased incoming airspeeds result in higher propeller rotational speeds. As the propeller's rotational speed rises, the frequency of the forward whirling mode increases, while the frequency of the backward whirling mode falls. This relationship is due to the difference in the sign of the gyroscopic term presented in Equation (19).

For further validation of the baseline propeller, a typical stability boundary curve was derived, as depicted in Figure 7. The attachment stiffnesses of the propeller pivoting point in pitch (K_θ) and yaw (K_ψ) were changed and the corresponding whirl flutter stability boundary curve was achieved for the whirl flutter speed of 223 m/s. As anticipated, the resulting curve, which shows the necessary stiffness to maintain stable dynamic behaviour, aligns with existing literature [23].

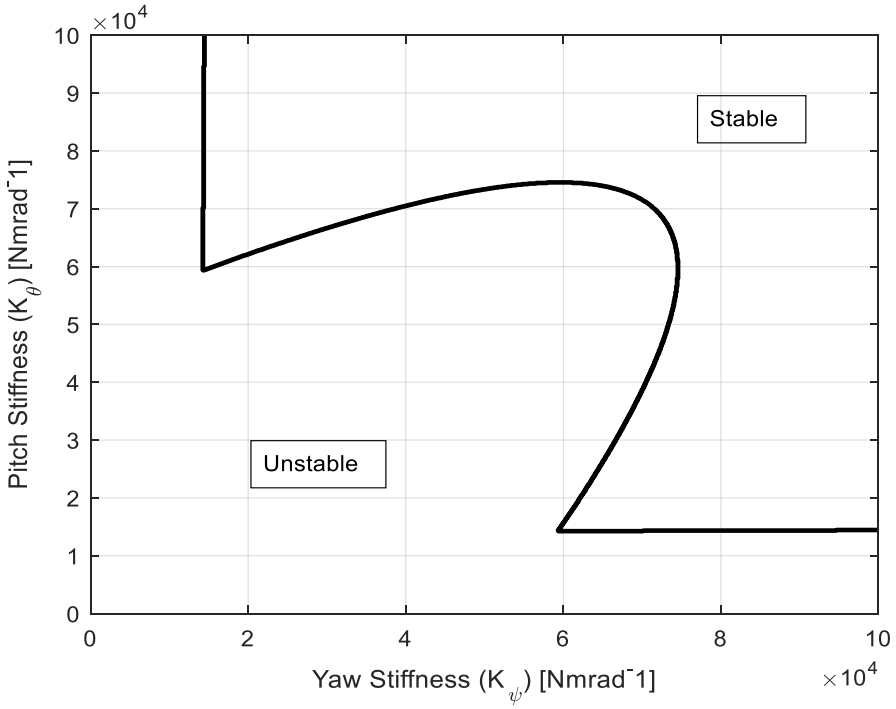

Figure 7: Stability boundary for baseline propeller model in the structural pitch stiffness K_θ and yaw stiffness K_ψ plane for a whirl flutter speed of 223 m/s

To determine the influence of variations in propeller parameters on stability boundary in the structural pitch stiffness K_θ and yaw stiffness K_ψ plane, parametric studies on the developed whirl flutter model of the baseline propeller are conducted. As can be seen from Figure 8, raising the freestream velocity *V,* the rotor's moment of inertia I_x, the nacelle's moment of inertia I_n and the rotor radius *R* expands the unstable region symmetrically. On the other hand, increasing the damping in both pitch and yaw *(C_θ, C_ψ)* and the advance ratio *J* reduces the unstable region symmetrically.

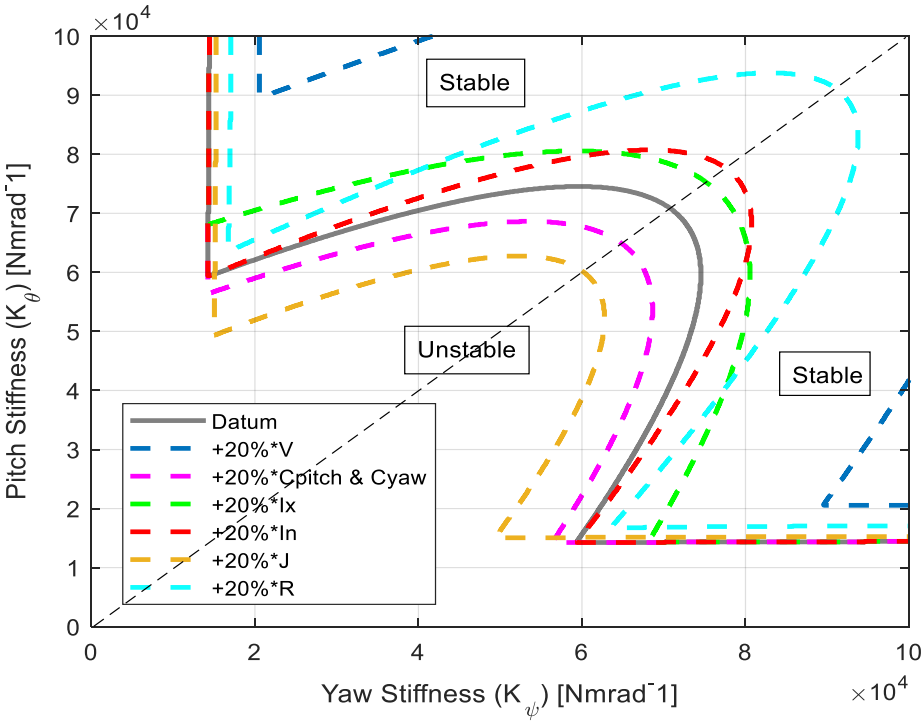

Figure 8: Effect of changes in some propeller parameters on stability boundary in the structural pitch stiffness K_θ and yaw stiffness K_ψ plane

The effect of the mounting stiffness on the whirl flutter velocity and frequency of the standalone propeller is investigated. It can be observed from Figure 9 that a higher mounting stiffness leads to a higher whirl flutter speed and frequency. As expected, this behaviour is in line with the literature [23].

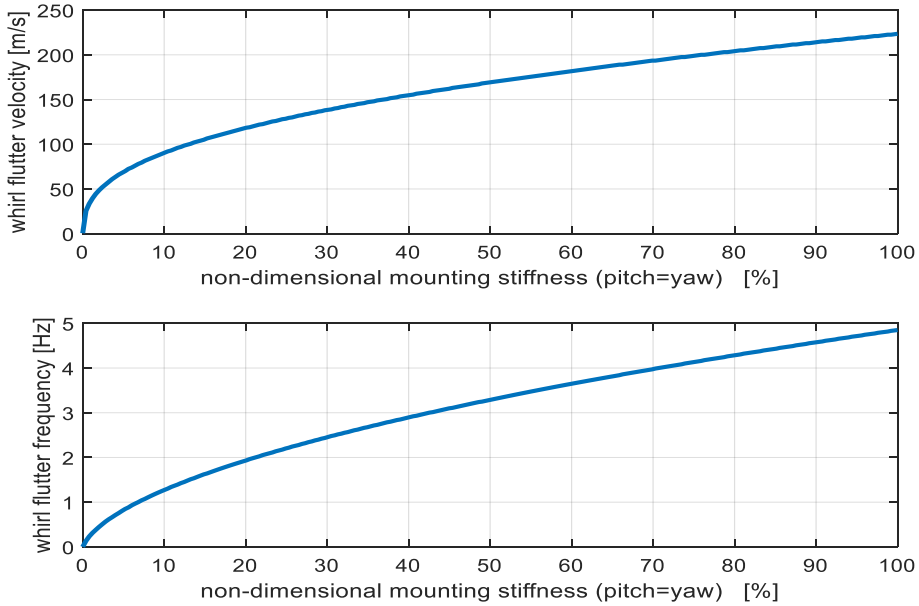

Figure 9: Effect of mounting stiffness of propeller on whirl flutter velocity and frequency

3.3 Coupled Wing-Propeller Model

The coupled wing-propeller model considered in this study consists of the baseline wing and propeller described in sections 3.1 and 3.2, respectively. The schematic of this coupled model is shown in Figure 10. The propeller is installed at a spanwise location of 31% from the wing root. The pivoting point of the propeller is located exactly on the elastic axis of the wing (the wing mid-chord axis). The propeller hub is situated 0.6 m from the leading edge, while the electric motor is positioned 0.3 m behind the propeller hub.

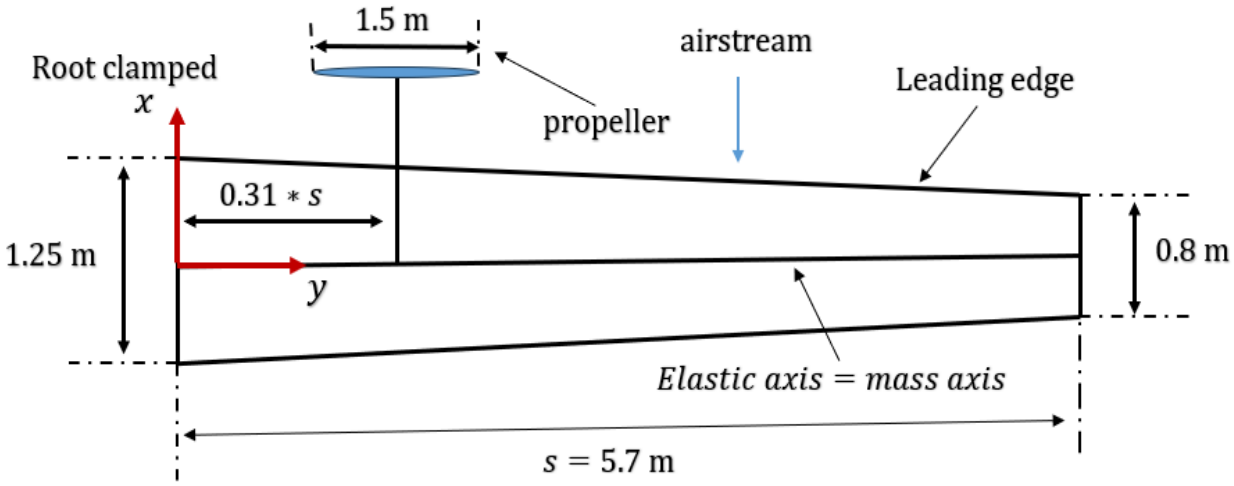

Figure 10: Schematic of the wing-propeller model

In the first setup, the effect of adding a non-rotating baseline propeller to the wing on the instability of the system is investigated. The non-rotating propeller model serves as a pylon and is rigidly attached to the wing, which means that the propeller mounts are assumed to be rigid. Hence, the added propeller changes the mass and inertial distributions of the wing. The second setup features a rotating propeller flexibly attached to the wing, enabling pitch and yaw movements and thus gyroscopic effects are included. Table 6 provides the natural frequencies of the rigidly-mounted propeller wing and the flexibly-mounted propeller wing models. It suggests that the whirling modes of the propeller are coupled with wing modes and this coupling largely depends on the uncoupled pitch and yaw frequencies of the propeller. Moreover, the pitch frequency of the propeller decreases as a consequence of the coupling between propeller pitch movement and wing torsion. However, the yaw frequency stays constant since the in-plane motions of the wing were not taken into account in this study. Additionally, it can be monitored that incorporating flexible mounts resulted in higher natural frequencies of the wing modes compared to the application of rigid mounts.

A rotating propeller introduces gyroscopic effects due to the presence of flexible mounts. To focus on the gyroscopic effects, propeller aerodynamics are ignored. Propeller rotational speed affects the propeller structural damping matrices and the propeller-wing coupling structural matrices. Figure 11 illustrates how increasing propeller rotational speed affects the natural frequencies of the propeller-wing system. The forward whirling mode frequency increases and the backward whirling mode reduces with increasing propeller rotational speed. These findings emphasize the importance of considering propeller whirling modes in the aeroelastic analysis of the DEP wings.

Table 6: Comparison of natural frequencies of the rigidly-mounted propeller wing and the flexibly-mounted propeller wing

Mode	Rigid Mounts and Non-rotating [Hz]		Flexible Mounts and Non-rotating [Hz]	
	Present Study	**Reference Study [13]**	**Present Study**	**Reference Study [13]**
First Bending	2.85	2.85	2.85	2.85
Propeller Pitch Mode	-	-	5.52	5.48
Propeller Yaw Mode	-	-	7	7
First Torsion	8.32	8.19	17.75	17.75
Second Bending	17.84	17.84	19.54	19.48
Second Torsion	26.31	26.23	49.29	49.25
Third Bending	49.98	49.98	51.34	51.37

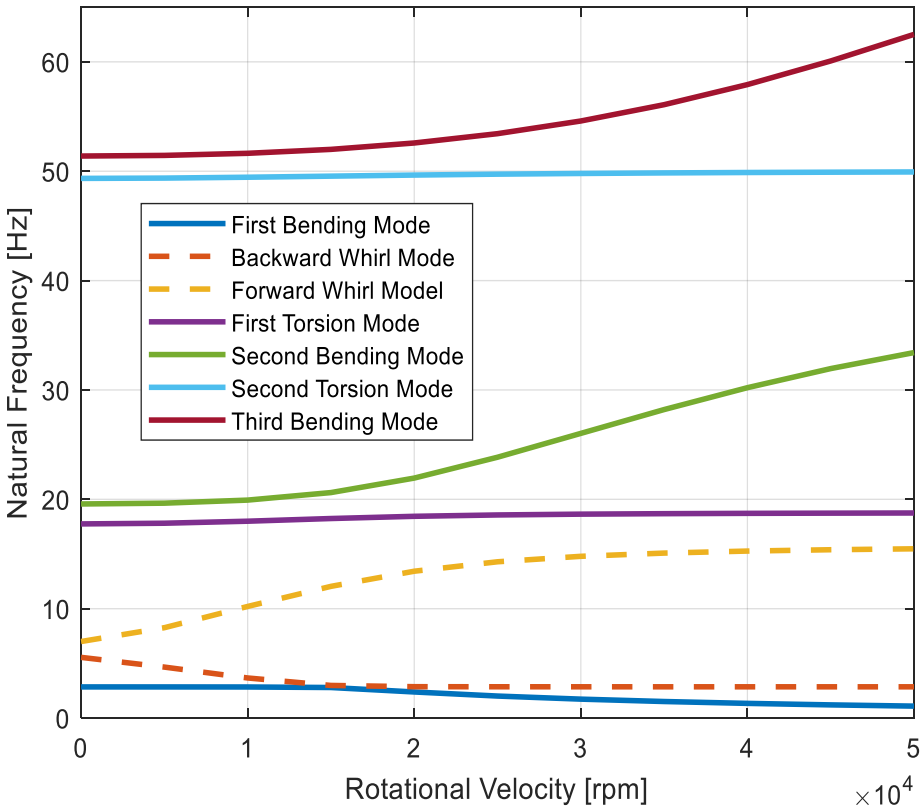

Figure 11: Influence of gyroscopic effects on natural frequencies of propeller-wing model

Table 7 outlines the aeroelastic results of the propeller-wing model with a rigidly attached propeller and a flexibly attached propeller. On the one hand, in the coupled propeller-wing configuration with a non-rotating propeller and rigid mounts, the propeller, acting as an inertial mass, decreased the flutter velocity compared to the baseline wing. On the other hand, in the case of the coupled propeller-wing configuration with a non-rotating propeller and rigid mounts, the propeller increased the flutter velocity compared to the baseline wing. Also, whirl flutter occurs in the forward whirling mode.

Table 7: Aeroelastic results of the rigidly and the flexibly-mounted propeller wings

Parameter	Rigid Mounts	Flexible Mounts
Wing Flutter Speed	125 m/s	202 m/s
Wing Flutter Frequency	6.40 Hz	2.79 Hz
Whirl Flutter Speed	-	302 m/s
Whirl Flutter Frequency	-	7.41 Hz

The velocity-damping and velocity-frequency curves of the propeller-wing model with both a rigidly mounted propeller and a flexibly mounted propeller are depicted in Figures 12 and 13.

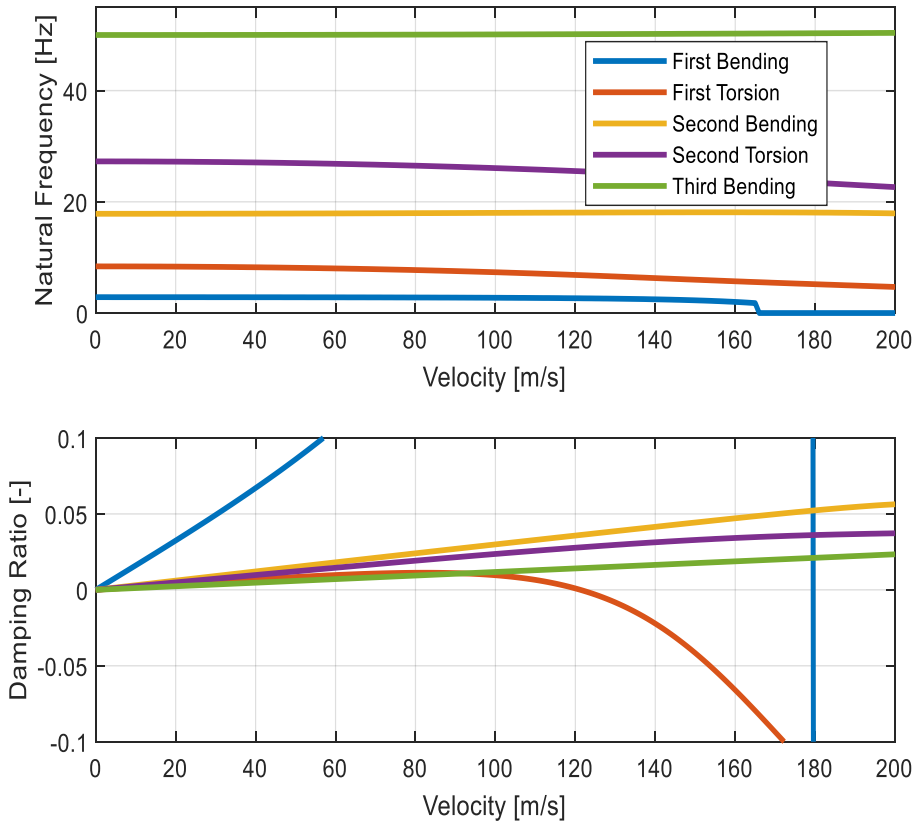

Figure 12: Variations of modal frequency and damping with freestream velocity for the coupled wing-propeller model with rigid mounts

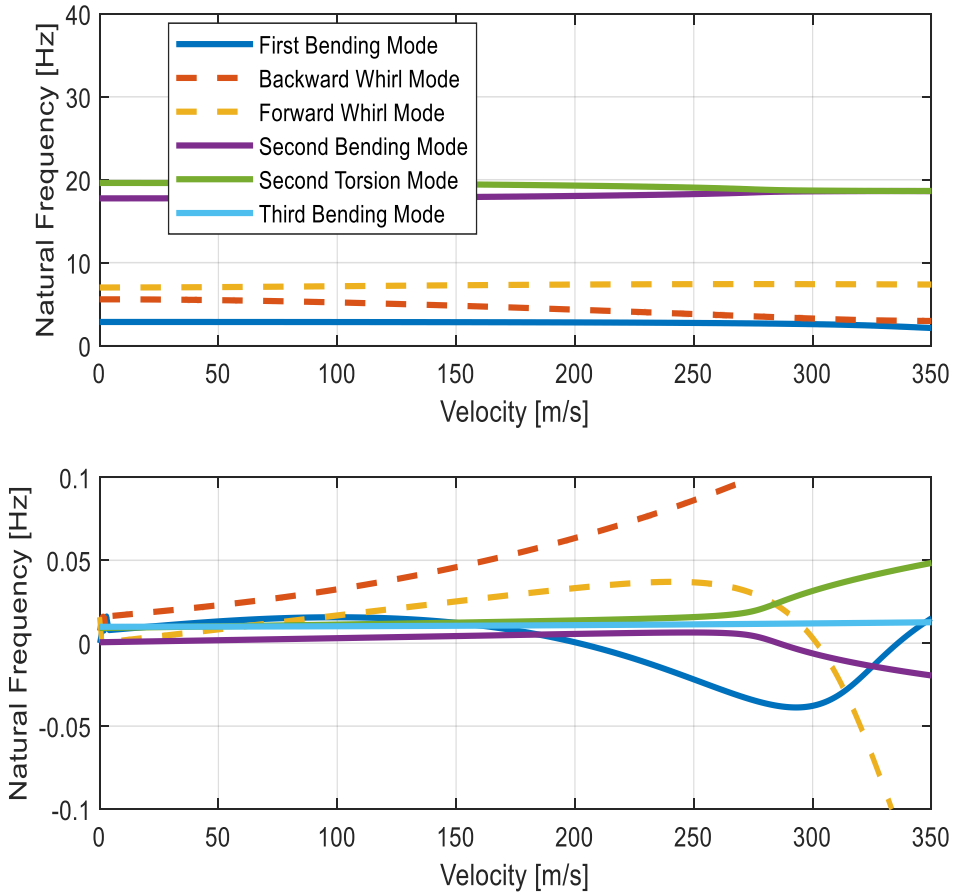

Figure 13: Variations of modal frequency and damping with freestream velocity for the coupled wing-propeller model with flexible mounts

3.4 Parametric Analyses

Several parametric analyses are carried out by changing the propeller's spanwise position, advance ratio and rotor radius, determining their impact on the stability of the coupled wing-propeller model defined in subsection 3.3. The first parametric analysis is undertaken by attaching the propeller to three different spanwise positions (a spanwise position of %31, a spanwise position of %70, and a spanwise position of %100). For this analysis, the same baseline wing and propeller are employed. The effect of each spanwise position of the propeller is evaluated on the stability of the coupled wing-propeller model. As shown in Figure 14, installing the propeller at the wingtip slightly affects the stability of the coupled model, decreasing the unstable region.

The second parametric analysis focuses on investigating the effect of three different advance ratios of the propeller on the stability of the coupled model. This study uses fixed-pitch propellers, where, under windmilling conditions, the propeller's rotational speed changes according to the incoming airspeed to maintain the advance ratio determined by the collective pitch angle. For the baseline isolated propeller, increasing the advance ratio has a stabilizing effect. This trend is illustrated in Figure 8 for the isolated propeller. However, for the coupled propeller-wing model, the variation of the advance ratio primarily affects the aerodynamics of the propeller and its gyroscopic

coupling. Increasing the advance ratio is destabilizing. This effect is depicted in Figure 15 for the coupled propeller-wing model.

The last parametric study is undertaken by varying the rotor radius in the coupled wing-propeller model. On the one hand, for the baseline isolated propeller, raising the rotor radius has a destabilizing effect, as depicted in Figure 8. On the other hand, it is observed from Figure 16 that raising the rotor radius has a stabilizing effect on the coupled model.

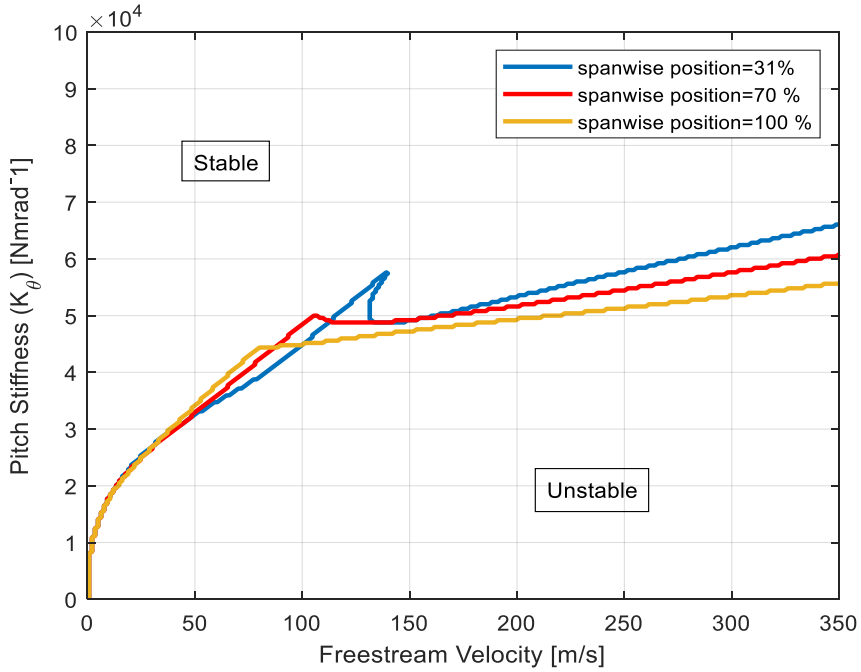

Figure 14: Effect of propeller spanwise position on the stability of coupled model

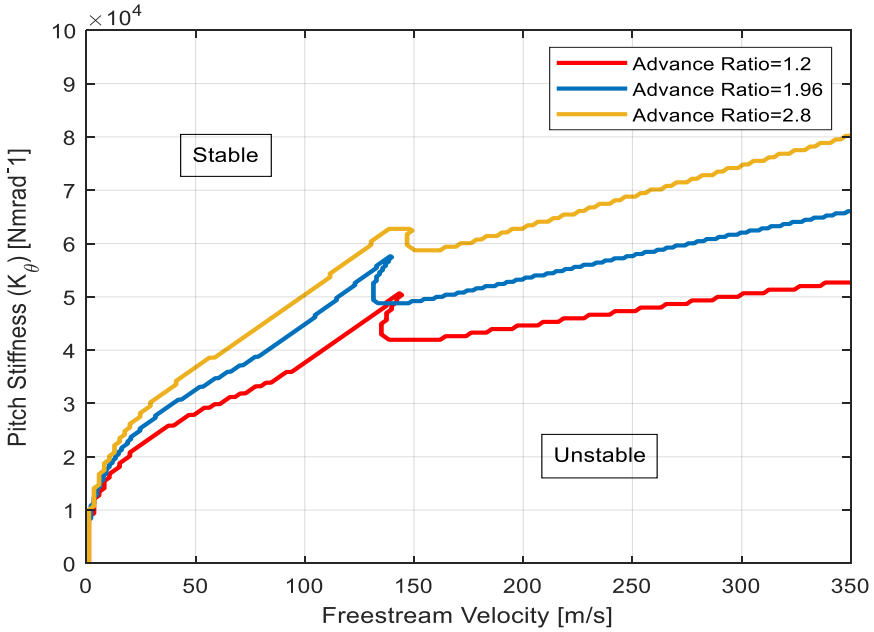

Figure 15: Effect of advance ratio on the stability of coupled propeller-wing model

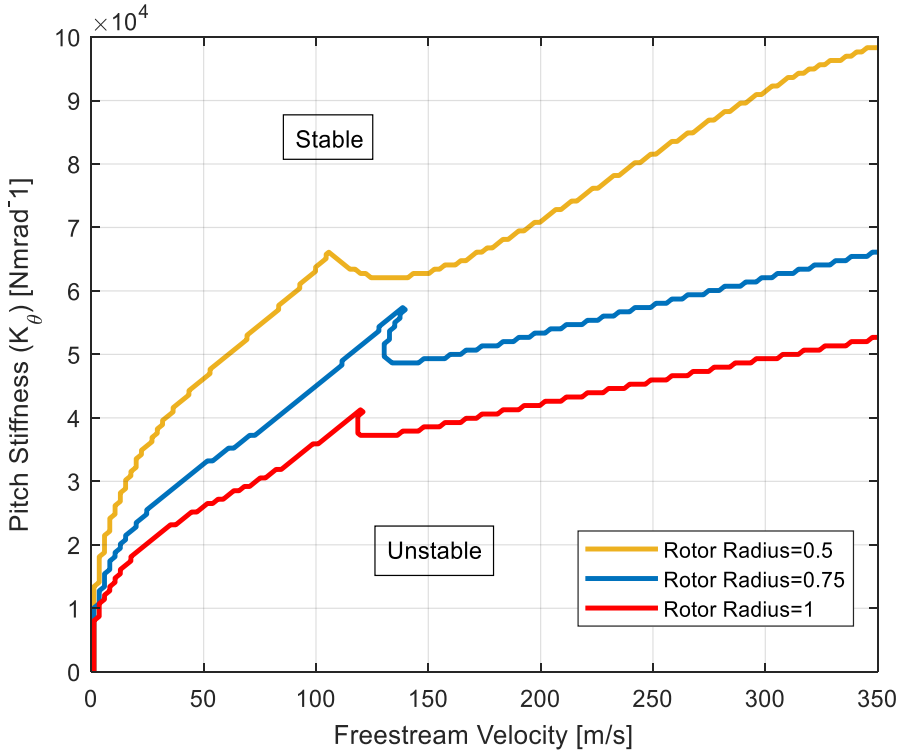

Figure 16: Effect of rotor radius on stability of coupled propeller-wing model

4 CONCLUSIONS

This paper focuses on developing a representative low-order aeroelastic coupled wing-propeller model that can be used during the preliminary design stages of DEP wings. A numerical aeroelastic model was created in MATLAB to investigate the aeroelastic behavior of a coupled flexible cantilever wing with a varying number of flexibly mounted propellers/rotors. Propeller dynamics are modeled using Reed's model, while the wing's structural model is derived using the assumed-mode Rayleigh-Ritz method. The wing's aerodynamic model is obtained by combining the modified strip theory and Theodorsen's unsteady aerodynamic theory. The proposed coupled aeroelastic model successfully predicted both wing and whirl flutter in DEP wings.

The baseline propeller used in this study involves fixed-pitch blades operating under windmilling conditions. Therefore, the propeller advance ratio remains constant and is determined by the specified geometric collective pitch angle. To maintain this advance ratio, the propeller's rotational speed varies with the freestream velocity. As expected, the gyroscopic effects cause the propeller hub to exhibit backward whirling motion at lower frequency modes and forward whirling motion at higher frequency modes. In the coupled propeller-wing configuration with a non-rotating propeller and rigid mounts, incorporating a non-rotating propeller decreased the critical speed in comparison to the baseline wing. In the case of involving a rotating propeller and flexible mounts, wing flutter increased compared to the baseline wing. The forward whirling mode led to a critical speed. Compared to the baseline isolated propeller, the backward whirling mode remains stable. However, the forward whirling mode, which is always stable in the baseline isolated propeller, becomes unstable due to wing aerodynamics.

The developed coupled model was subsequently applied onto parametric analyses identifying the impact of propeller spanwise position, advance ratio and rotor radius on the stability of the coupled wing-propeller system. The results of parametric studies indicated that advance ratio and rotor radius have a significant impact on the stability of the coupled wing-propeller model, whereas the spanwise position of the attached propeller has a slight effect. As the advance ratio of the attached propeller rises, a destabilizing effect on the stability of the coupled model is monitored. It was also observed that increasing rotor radius has a stabilizing effect on the stability of the coupled wing-propeller model.

The presented study shows how rapidly the proposed coupled aeroelastic model can be modified in various parametric studies that can be performed during the preliminary design stages of the DEP wings. The current investigations are limited to a wing-propeller model with one inboard propeller. Future studies should focus on a DEP aircraft wing configuration with multiple propellers and additional parameters, such as their chordwise position and mounting stiffness. Furthermore, the physical model should be enhanced to account for aerodynamic interference effects between the propeller and wing aerodynamics.

REFERENCES

[1] Nguyen, N.T., Reynolds, K., Ting, E., et al. (2018). Distributed propulsion aircraft with aeroelastic wing shaping control for improved aerodynamic efficiency. *Journal of Aircraft,* 55, 1122-1140.

[2] Brelje, B. J. and Martins, J. R. R. A. (2019). Electric, hybrid, and turboelectric fixed-wing aircraft: A review of concepts, models, and design approaches. *Progress in Aerospace Sciences*, 104, 1–19.

[3] Moore, J. B. and Cutright, S. (2017). Structural design exploration of an electric powered multi-propulsor wing configuration. In *58th AIAA/ASCE/AHS/ASC Structures, Structural Dynamics, and Materials Conference*. p. 203.

[4] NASA. https://www.nasa.gov/image-detail/x-57_maxwell_city_0/, (accessed April 25, 2024).

[5] DLR. https://www.dlr.de/en/latest/news/2021/04/20211215_towards-zero-emission-aviation, (accessed April 25, 2024).

[6] Rotundo, C., Jinks, E., and Öngüt, E., (2023). Whirl flutter analysis across multiple configurations: Preprocessor implementation and verification. In *Royal Aeronautical Society 8th Aircraft Structural Design Conference*.

[7] Reed, W.H. and Bland, S.R. (1961). An analytical treatment of aircraft propeller precession instability. *NASA Technical Note,* p. 659.

[8] Houbolt, J. C. and Reed, W. H. (1962). Propeller-nacelle whirl flutter. *Journal of the Aerospace Sciences*, 29(3), 333–346.

[9] Bland, S. R., and Bennett, R. M. (1963). Wind-tunnel measurement of propeller whirl-flutter speeds and static-stability derivatives and comparison with theory. *Langley Research Center, Washington, USA Technical Note D-1807.*

[10] Bennett, R. M., and Bland, S. R. (1964). Experimental and analytical investigation of propeller whirl flutter of a power plant on a flexible wing. *NASA Technical Note D-2399.*

[11] Rodden, W. P. and Rose, T. L. (1989). Propeller/nacelle whirl flutter addition to

MSC/NASTRAN.

[12] Reed III, W.H. (1966). Propeller-rotor whirl flutter: A state-of-the-art review. *Journal of Sound and Vibration*, 4(3), 526–544.

[13] Liu Xu, V. Q. (2020). *Propeller-wing whirl flutter: An analytical approach*. Master's Thesis, Delft University of Technology.

[14] Amoozgar, M., Friswell, M. I., Fazelzadeh, S. A., et al. (2021). Aeroelastic stability analysis of electric aircraft wings with distributed electric propulsors. *Aerospace*, 8(4),100.

[15] Heeg, J., Stanford, B. K., Kreshock, A., et al. (2019). Whirl flutter and the development of the NASA X-57 Maxwell. In *International Forum on Aeroelasticity and Structural Dynamics*, NF1676L-31615.

[16] Böhnisch, N., Braun, C., Koschel, S., et al. (2022). Whirl flutter for distributed propulsion systems on a flexible wing. In *AIAA SCITECH 2022 Forum*. p. 1755.

[17] Böhnisch, N., Braun, C., Koschel, S., et al. (2022). Dynamic aeroelasticity of wings with distributed propulsion system featuring a large tip propeller. In *International Forum on Aeroelasticity and Structural Dynamics*, Madrid, Spain.

[18] Böhnisch, N., Braun, C., Muscarello, V., et al. (2023). A sensitivity study on aeroelastic instabilities of slender wings with a large propeller. *AIAA SCITECH 2023 Forum*. p. 1755.

[19] Tamer, A. and Tatar, A. (2023). A minimum complexity model for the aeroelastic analysis of distributed propulsion aircraft. In *the European Rotorcraft Forum.*

[20] Wright, J. R. and Cooper, J. E. (2007). *Introduction to Aircraft Aeroelasticity and Loads*. CBS Publishers & Distributers.

[21] Bielawa, R.L. (2006). *Rotary Wing Structural and Aeroelasticity.* American Institute of Aeronautics & Astronautics, Washington.

[22] Mair, C., Rezgui, D., and Titurus, B. (2018). Nonlinear stability analysis of whirl flutter in a rotor-nacelle system. *Nonlinear Dynamics*, 94(3), p. 2013-2032.

[23] Cecrdle, J. (2015). *Whirl Flutter of Turboprop Aircraft Structures.* United Kingdom: Woodhead Publishing.

ACKNOWLEDGEMENT

This study was funded by the Ministry of National Education of the Republic of Turkey under YLSY grant.

COPYRIGHT STATEMENT